Experimental Investigation on Combination of Soil Electrokinetic Consolidation and Remediation of Drained Water Using Composite Nanofibers-Based Electrodes

Samar Behrouzinia[a], Hojjat Ahmadi[b*], Nader Abbasi[c], Akbar A. Javadi[d]

a- Ph.D. Graduated in Hydraulic Structures, Department of Water Engineering, Urmia University, IRAN

b- Associate Professor, Department of Water Engineering, Urmia University, IRAN

c- Professor, Agricultural Engineering Research Institute, Agricultural Research, Education and Extension Organization, (AREEO), Karaj, Iran

d- Professor, Department of Engineering, College of Engineering, Mathematics and Physical Sciences, University of Exeter, North Park Road, Exeter EX4 4QF, UK

*-corresponding author: h.ahmadi@urmia.ac.ir

Abstract

A novel electrokinetic geosynthetic (EKG) can be efficient in achieving multiple objectives. In this study, a new EKG as an electrode and a drainage channel in the electro-osmotic consolidation was fabricated by electrospun nanofibers containing graphene nanoparticles (GNs) attached to a carbon fiber substrate. To investigate the effectiveness of the fabricated electrodes in electro-osmotic consolidation and remediation of water drained from the system, an experimental apparatus was constructed with given considerations such as the loading capability in expanded ranges and application of the electric field and filled with copper-contaminated kaolinite. Experiments were divided into two groups, control and EKG experiments. All the experiments were carried out with the same conditions, loading, drainage condition, and duration. However, EKG experiments were performed with the application of the electric field under the vertical pressure in the range of 7-113 kPa, and the control experiment was conducted without the application of the electric field. According to experimental results, 18 wt% polymethyl methacrylate (PMMA) in the DMF solvent containing 1 and 2 wt% GNs was selected to make a nanofibrous layer on the carbon fiber. The average diameters of the fibers were 404 ± 36 and 690 ± 62 and yielded at 1 and 2 wt% GNs, respectively. The results showed that using the electrokinetic geosynthetic accelerated the consolidation of the kaolinite. The average degree of consolidation was 68% in the control experiment and 85% in the EKG experiments. Furthermore, the fabricated electrodes were very effective as a drainage channel to remediate water drained from the system. The highest copper removal efficiency was obtained in ES_2-EK (97%) and ES_1-EK (92%), respectively. The lowest copper removal efficiency was obtained in C-EK (85%).

Keywords: Carbon Fiber, EKG, Electrospinning, Graphene, PMMA, Removal

1. Introduction

Dependency between electrical flows and gradients as well as hydraulic flows and gradients can induce different electrokinetic (EK) phenomena in fine-grained soils (Mitchell and Soga 2005). The four main phenomena occurred by electrokinetic are electroosmosis (induced water flow due to electrical gradient), electrophoresis (induced particle movement due to electrical gradient), streaming potential (electrical potential due to water flow), and migration or sedimentation potential (electrical potential due to particle movement).

Because electrokinetic can be an environmentally friendly (lower environmental effect compared with others) and economically viable method, it is a useful technique to improve the soils (Eriksson and Gemvik 2014). Therefore, most studies have focused on three main applications related to electrokinetic, electrokinetic consolidation (EKC) for improving the engineering properties of the soft clays and accelerating the process of soil consolidation (Malekzadeh et al. 2016; Azhar et al. 2017), electrokinetic dewatering (EKD) for minimizing the sludge volume, facilitating transportation, and reducing leachate production in sludge landfill sites (Cao et al. 2020; Wu et al. 2020), and electrokinetic remediation (EKR) for removing inorganic, organic pollutants or reducing their toxicity (Dos Santos et al. 2020).

Electrokinetic efficiency and durability are significantly affected by the electrode materials due to energy dissipation induced by voltage loss and chemical reactions at the soil-electrode interface (Mohamedelhassan and Shang 2001; Zhou et al. 2015). Electrode materials used in electrokinetic applications can be divided into two groups, traditional and modern materials.

Traditional electrodes widely used with different approaches, including iron electrodes applied for EKC (Hu et al. 2013; Fu et al. 2018; Yang et al. 2021) and EKD (Bayat et al. 2006; Fu et al. 2019), copper electrodes used for EKC (Bergado et al. 2003; Zhuang and Wang 2007; Badv and Mohammadzadeh 2015) and EKR (Behrouzinia et al. 2021), steel electrodes used for EKD (Qian et al. 2019; Wu et al. 2019; Malekzadeh and Sivakugan 2021; Rotte et al. 2021), EKR (Cappello et al. 2019; Czinnerová et al. 2020), and EKC (Burnotte et al. 2004; Deng and Zhou 2016; Wang et al. 2016; Fu et al. 2017; Zhang et al. 2017; Wang et al. 2018; Yang et al. 2021; Zhang et al. 2021), aluminium electrodes used for EKC (Wang and Vu 2010), titanium electrodes used for EKD (Ahmad et al. 2006; Otsuki et al. 2007; Rao et al. 2021), and graphite (or carbon) electrodes used for EKD (Rao et al. 2021), EKR (Altin and Degirmenci 2005, Ramírez et al. 2015; Peppicelli et al. 2018; Cai et al. 2021; Ghobadi et al. 2021; Xu et al. 2021), and EKC (Bergado et al. 2003; Flora et al. 2017; Hu et al. 2019).

Modern electrodes were introduced to suppress the electrochemical dissolution of the anode. Therefore, lead oxide, gold, and platinum, very expensive, were mentioned by Mahmoud et al. (2010). Besides, mixed metal oxide (MMO) electrodes, also called dimensionally stable anodes (DSA), were used as anodes in applications related to EKD (Mahmoud et al. 2011; Olivier et al. 2015; Mahmoud et al. 2016; Mahmoud et al. 2018; Cao et al. 2019; Zhang et al. 2021) and EKR (Chowdhury et al. 2017). The DSA electrodes were made by coating a substrate, such as a pure titanium plate or expanded mesh, with several kinds of metal oxides such as iridium

oxide, in EKD (Lee et al. 2016; Guo et al. 2017; Li et al. 2018) and EKR (Cappello et al. 2019), and ruthenium oxide, in EKD (Citeau et al. 2011). Concerning making corrosion-free electrodes, electrokinetic geosynthetic (EKG) materials were achieved by coupling electrokinetic with traditional functions of geosynthetics (Jones et al. 2014).

EKGs (or electrically conductive geosynthetics) are fabricated by the addition of conductive elements to geosynthetics or conventional polymers using weaving, knitting, needle punching, and extrusion or laminating techniques, and they can be in 2D or 3D shapes (Lamont-Black et al. 2015). Electrokinetic vertical drains (EVDs), used in consolidation by Chew et al. (2004); Karunaratne et al. (2004); Rittirong et al. (2008); Kaniraj and Yee (2011); Kaniraj et al. (2011); Kaniraj (2014); Wang et al. (2020) and strengthening of soft clay by Sun et al. (2021), or electrokinetic prefabricated vertical drains (ePVDs), used in consolidation by Liu et al. (2014); Zhuang et al. (2014); Shen et al. (2019); Zhang and Hu (2019); Hu et al. (2020); Zhuang (2021) and stabilization of embankment and soft clay by Lamont-Black et al. (2012); Azhar et al. (2018), respectively, are types of commercially accessible EKG electrodes. Other kinds of EKG electrodes were developed through interlacing metal filament in the geotextile (such as copper wires in the polyester cotton for dewatering (Patel et al. 2021), steel wires in the textile for stabilization of slopes (Mumtaz and Girish 2014), and titanium wires coated with the mixed metal oxide layer in a polyester woven filter for dewatering of tunneling slurry waste (Kalumba et al. 2009)) and coating a metal core (such as a graphite sheet inside two layers of perforated Perspex sheets for isolation of cadmium (Tang et al. 2018) and a metal sheet surrounded in an electrically conductive polymer for dewatering of mine tailings (Fourie and Jones 2010)). Besides, EKG electrodes can be made from composite materials, which have at least an electrically conductive component, such as electrokinetic geocomposites (eGCP) fabricated to dewater fluid fine tailings (Bourgès-Gastaud et al. 2015) and oil sand tailings (Bourgès-Gastaud et al. 2017). Different shapes of EKG electrodes are geonet and EKG bags used for dewatering of mine tailings (Fourie et al. 2007) and nuclear contaminated waste (Lamont-Black et al. 2015). Carbon fiber plate and a drainage pipe wrapped with carbon fiber are other novel types of EKG electrodes used to consolidate clayey soils (Gargano et al. 2019) and dewater subgrade soil (Ling et al. 2021), respectively.

According to the literature review, in which the most important electrokinetic applications using traditional and modern electrodes in complicated geotechnical problems were investigated, the electrodes were improved to reduce corrosion and increase durability and placed in the soil only as conducting elements. In this study, through adding an innovative capability related to metal removal to the structure of electrodes, a novel EKG electrode as an electrode and a drainage channel was designed to consolidate kaolinite and remediate the copper contaminated water drained from the system, simultaneously. New EKG electrodes were fabricated by electrospun nanofibers containing graphene nanoparticles (electrospun composite nanofibers) attached to a substrate layer, carbon fiber. To investigate the effectiveness of the fabricated EKG electrodes in electro-osmotic consolidation and remediation of water, an experimental apparatus was constructed, and the results of the

electrokinetic experiments were analyzed in comparison with the control experiment (without applying DC voltage).

2. Materials and Methods

2.1. Preparation of soil specimens

Commercial kaolinite was used as a base soil material in this study. The soil's chemical compositions, mineralogical compositions, and other physical properties were shown in Tables 1 and 2, respectively. Contaminated material was made by mixing the kaolinite with copper chloride after it was dried at 105 °C for 24 hours. According to Yip et al. (2009), the competitive sorption of metals can change their distribution in the different sections of the soil and for this very reason, we used artificially contaminated soil to assess the role of fabricated EKG electrodes in the soil consolidation and remediation of water drained from the system. Based on the Government Decree on the Assessment of Soil Contamination and Remediation Needs 214/2007 (MEF 2007), the copper threshold in the soil is 100 mg/kg. and on the other hand, the world average copper concentration in the soil is 30 mg/kg (Ballabio et al. 2018). The initial concentration of copper was considered 200 mg/kg, in which most of the copper is kept by the soil matrix (Chen et al. 2011).

The water content of the sample should be enough to allow the occurrence of the electro-osmotic flow. Approximately 1.5 times the kaolinite liquid limit was used to saturate the soil according to the recommendations (Hamir et al. 2001; Karunaratne et al. 2004; Chien et al. 2009). Sodium chloride salt in the concentration of 2 g/L was added to the sample to improve the electrokinetic process (Micic et al. 2001; Eriksson and Gemvik 2014).

Table 1

Chemical properties of the kaolinite.

Composition	Value	Composition	Value
Chemical compositions (X-ray diffraction)			
Ignition loss (%)	8.5±1	Calcium oxide (%)	1.5±0.2
Silicon dioxide (%)	65±1	Magnesium oxide (%)	0.35±0.05
Aluminium oxide (%)	22±1	Sodium oxide (%)	0.35±0.05
Iron (III) oxide (%)	0.75±0.1	Potassium oxide (%)	0.25±0.05
Titanium dioxide (%)	0.04±0.01		
Anionic compositions (Titration method according to Page et al. 1982)			
Sulfate (meq/L)	1.40		
Chloride (meq/L)	2.5		
Bicarbonate (meq/L)	6.25		

Table 2

Mineralogical compositions and properties of the kaolinite.

Parameter	Value	Parameter	Value
Mineralogical Analysis (X-ray diffraction)		Atterberg limits (ASTM D 4318)	
Kaolinite (%)	60±2	Liquid limit (%)	41
Quartz (%)	31±2	Plastic limit (%)	32
Calcite (%)	2.5±0.5	Plasticity index (%)	9
Total Feldspar (%)	-		
Others (%)	6±1	Specific gravity (ASTM D 584)	2.54
Particle Size Distribution		USCS classification (ASTM D 2487)	ML
> 40μ (%)	0-0.5	pH (ASTM D 4972)	7.82
< 20μ (%)	98		
< 2μ (%)	39±3		

2.2. Fabrication of EKG electrodes

In this study, to carry out electro-osmotic consolidation and remove copper metal during the process, novel electrokinetic geosynthetic electrodes in a range of environmental protections were designed. The EKG electrodes consisted of carbon fiber and composite nanofibers. The plain carbon fiber, which created a grid-like pattern and was a slightly tighter weave pattern than twill, was considered as a substrate layer of electrodes. The composite nanofibers electrospun by electrospinning technique contained graphene nanoparticles and were added to the structure of the EKG electrode.

The unique characteristics such as high specific surface area and high porosity (Najafabadi et al. 2015), strong surface adhesion and surface flexibility (Lu and Ding 2008), tunable structures, and simple chemical modifications (Zhang et al. 2020) made nanofibers so efficient to enhance the removal. Therefore, the nanofibrous structure as an effective layer of EKG electrodes fabricated was used to improve the metal removal from the drained water of the system.

2.2.1. Substrate of EKG electrodes

As recommended by Pugh (2002) about the required properties in the electrodes, carbon fiber can be introduced and used as one of the most efficient geosynthetic electrodes due to its suitable electrical and structural properties (Table 3). This study applied carbon fibers with an average diameter of 7 μm (Fig. 1). The carbon fiber made of polyacrylonitrile polymer contains 93% carbon. And, the mentioned carbon fibers have an electrical resistance of 1.7×10^{-5} Ω. m, which is about 100 times less than the electrical resistance (10^{-3} Ω. m) recommended by Zhuang et al. (2014) to conduct the electrokinetic process. On the other hand, carbon fibers can be used in various applications (such as EKG electrodes, electrode substrates, and drainage channels)

due to their properties, acid corrosion resistance, oxidation resistance, and the possibility of drainage within the fiber structure.

Table 3
Specifications of carbon fiber.

Specification	Examination Method	Unit	Examination Result
Tensile Strength	TY-030B-01	MPa	3530
Tensile Strength	TY-030B-01	GPa	230
Strain	TY-030B-01	%	1.5
Density	TY-030B-02	g/cm^3	1.76
Filament Diameter	-	µm	7
Thermal Conductivity	-	Cal/cm.s.°C	0.025
Electrical Resistivity	-	Ω. m	1.7×10^{-5}
Chemical Composition:			
Carbon	-	%	93
Na + K	-	ppm	< 50

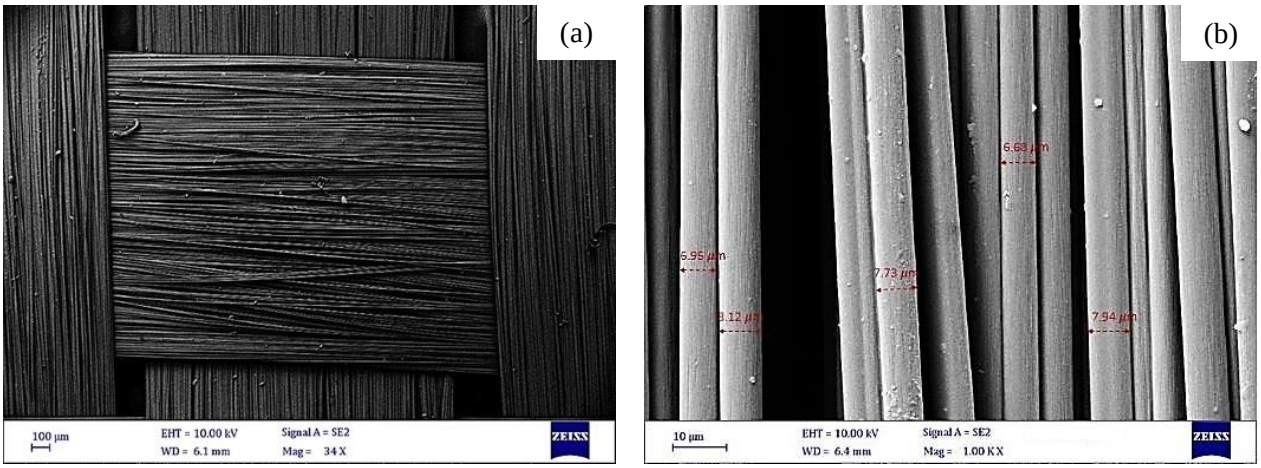

Fig. 1. Field emission scanning electron microscopy of carbon fiber (a) 100 µm, (b) 10 µm

2.2.2. Polymer, Solvent

To fabricate fibers using the electrospinning technique, solutions were prepared by dissolving 13, 15, and 18 wt% polymethyl methacrylate (PMMA, (–CH_2C–(CH_3) CO_2CH_3)–)) with a molecular weight (M_w) of 120 000 g/mol from Aldrich (Table 4) in N, N-dimethylformamide (DMF) solvent.

Table 4
Properties of polymethyl methacrylate (PMMA).

Specification	Examination Method	Unit	Result
Specific Gravity	ASTM D792	g/cm^3	1.188
Molar Mass	-	g/mol	120000
Tensile Strength	ASTM D638	Kg/cm^2	720
Tensile Elongation	ASTM D638	%	5
Flexural Strength	ASTM D790	Kg/cm^2	1100
Light Transmission	ASTM D1003	%	92
Izod Impact Strength (notched)	ASTM D256	Kg-cm/cm	2
Melt Flow Index	ASTM D1238	g/10min	1.8
Hardness	ASTM D785	M scale	95
Vicat Softening Temp.	ASTM D1525	℃	113
Heat Distortion Temp.	ASTM D648	℃	100

2.2.3. Graphene nanoparticle

In this study, graphene nanoparticles (Table 5) were utilized as nanofillers in electrospinning solutions. According to Fig. 2, the used graphene nanoparticles (GNs) had layered structures, and their diameters were in the range of 15-36 nm. To fabricate fibers using electrospinning, the weight percentage of graphene ranged between 1 and 3 wt%.

Table 5
Properties of graphene nanoparticles (GNs).

Specification	Unit	Value	Specification	Unit	Value
Bulk Density	g/cc	0.08	Number of Layers	-	2-5
Diameter Average X & Y Dimensions	micron	1-2	Surface Area	m^2/g	300
Thickness Average Z Dimension	nm	3-6	Tensile Modulus	Gpa	> 1000
Carbon Purity	%	98 >	Tensile Strength	Gpa	> 5
Oxygen Content	%	< 2	Termal Conductivity	S/m	10^7

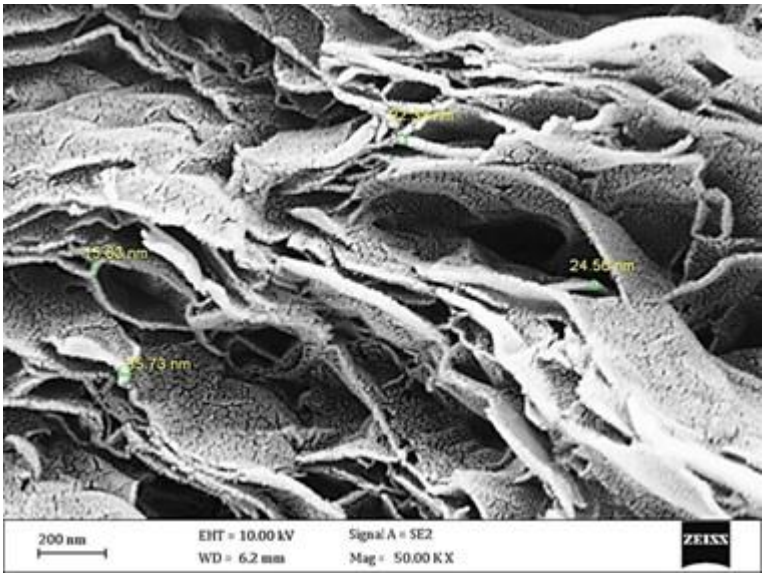

Fig. 2. Field emission scanning electron microscopy of graphene nanoparticles

2.2.4. Preparation of electrospinning solution

Electrospinning is a method used for producing continuous nonwoven fibers, and their diameters range from micrometers to several nanometers. Because of some advantages such as convenient operation and ability to control fiber diameter (Li et al. 2014), diversity of materials used for electrospinning (Lu and Ding 2008), low-cost apparatus, a possibility to mass production (Tan et al. 2007), and minimum solution consumption (Thenmozhi et al. 2017), the electrospinning technique is widely used for both academic and industrial projects (Zhang et al. 2020), and its main principle is electrostatic interactions (Thenmozhi et al. 2017). The electrospinning system consists of 3 major parts: a liquid feeding system for delivering the solution at a constant flow rate, a high voltage power source, and a collector installed either vertically or horizontally.

To prepare the uniform and homogenous electrospinning solution containing nanofillers, the different weight percentages of graphene nanoparticles, 1-3 wt%, were dispersed in DMF and sonicated for 60 min at room temperature. Then, a suitable PMMA concentration was added to the previous solution and dissolved for 24h. Finally, the obtained solution was sonicated at 50 ℃ for 30 min. The solution was injected into a 10-ml solution reservoir. The flow rate was 1 ml/h, and the distance between needle tip and drum was 15cm. The voltages applied during electrospinning were in the range of 15kV to 20kV. To fabricate EKG electrodes, electrospinning was performed for 2h on the substrate, carbon fiber. To assess the impacts of the electrospinning parameters, polymer and nanoparticles concentrations, on the morphology of fibers, the fabricated fibers were characterized by field emission scanning electron microscopy (FE-SEM).

2.3. Experimental apparatus

2.3.1. Loading system

In this study, a hydraulic shop press, purchased from Torin BIG RED, was used as a loading system with the following specifications: Model number= TY20001, capacity= 20 tons, weight= 96.8 kg, stroke= 185 mm, work range= 0-910 mm. The shop press has a heavy-duty H frame and consists of a pressure gauge, hydraulic pressure pump, press cylinder, and press bed frame.

To monitor the loads applied by the shop press and calibrate the pressure gauge of the shop press during experiments, a compression load cell with a capacity of 10 kN and sensitivity of 1.5 mV/V was used. At first, the load cell was calibrated (Fig. 3(a)) by using standard weight plates up to 20% of the nominal capacity of the load cell.

To record the output voltages due to the loading and calibrate the load cell, a data acquisition system (DAQ) was utilized and connected to the load cell in the loading system. The data acquisition system, Data Shuttle/USB 56, was a personal daq/50 series with 20 analog input ports and 16 digital input ports. The voltage applied to the data shuttle by a 12V power supply was 3 volts.

Because of loading in expanded ranges, a tonnage gauge can not be efficient in low pressures. So, a 14 bar pressure gauge was attached to the loading system, in addition to the tonnage gauge. It is required for the 14 bar pressure gauge to be calibrated, as well. Fig. 3(b) shows the calibration curve of the 14 bar pressure gauge in the ranges between 1.6 and 12 bar.

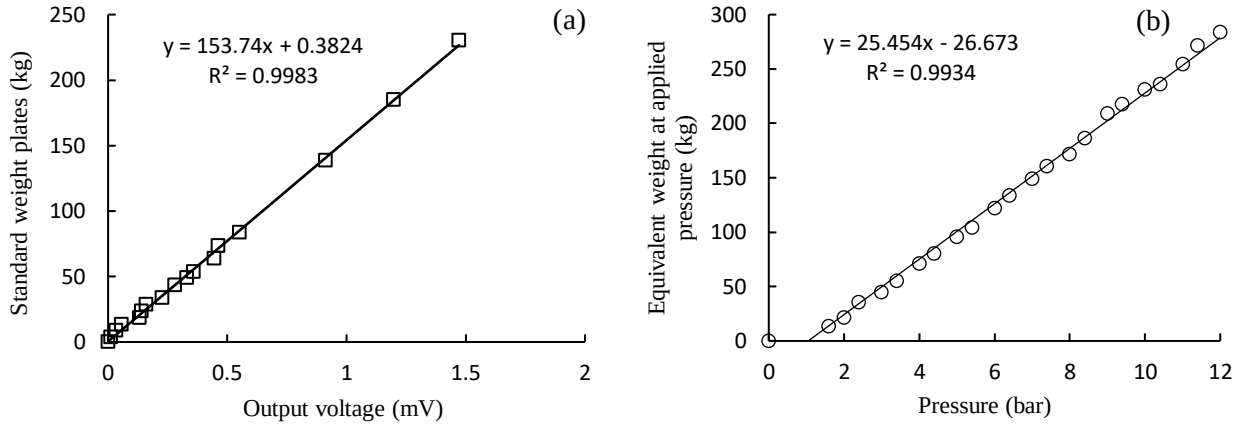

Fig. 3. Calibration curve (a) load cell, (b) pressure gauge

Loading in experiments was performed in the range of 7 to 113 kPa by the loading system (Fig. 4). Then, using the load cell placed between the press cylinder and the loading plate, a certain load in each time step was applied, and its fluctuations were controlled by the data shuttle recording the output voltage.

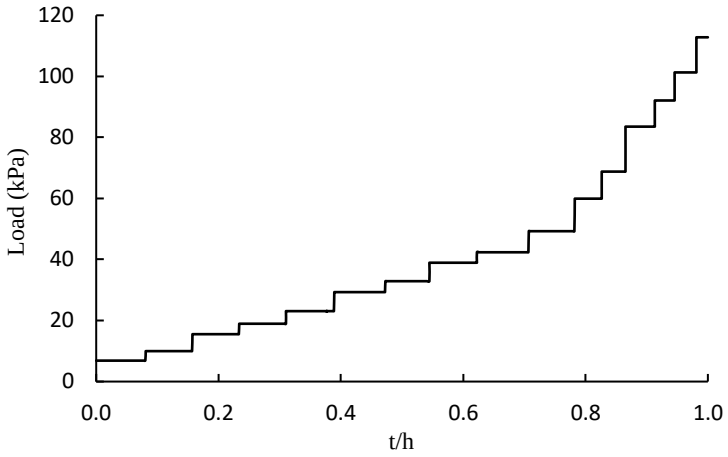

Fig. 4. Applied loads in time-steps

2.3.2. EK cell

In this study, a system, including the EK cell, loading system, and devices, was designed to carry out electrokinetic geosynthetic consolidation and remove copper metal from the drained water, as shown in Fig. 5. A rectangular chamber with external dimensions of 33(L) × 12(W) × 25(H) cm was made of Plexiglas in different thicknesses. The location of the soil chamber with internal dimensions of 25(L) × 10(W) × 20(H) cm was in the middle, where the anode and cathode electrodes were placed on both sides (Micic et al. 2001). Likewise, two chambers of anolyte and catholyte with dimensions of 2(L) × 12(W) × 25(H) cm were installed next to the anode and cathode electrodes and at the two end sides of the model. To monitor the voltage changes between the electrodes, four sensors were placed in the middle line of the model and at distances of 10, 75, 173, and 238 mm from the anode electrode. Two drainage valves at the ends of the cell were used to expel the water from the system. Due to applying the open cathode-closed anode boundary conditions, flow caused by electroosmosis migrated from anode to cathode, and it was collected by a graduated cylinder placed under the catholyte chamber. To expel the gases produced during the electrokinetic process, pores were considered in the upper surface of the anolyte and catholyte chambers. By placing a layer of geomembrane between the soil sample and the loading plate, drainage was accomplished only from both sides of the electrodes, and the drainage path was eliminated through the upper surface of the model. Therefore, the electro-osmotic flow was horizontally established in one dimension. A rectangular loading plate weighing 2.8 kg (in dimensions of 24(L) × 9.8(W) cm) was made and placed on the top of the soil sample. Assuming the occurrence of uniform settlement, a dial gauge was installed on the top of the soil to record the settlement during experiments. The electric field in the electrokinetic experiments was established by a 30 Volt 5 Amp DC power supply.

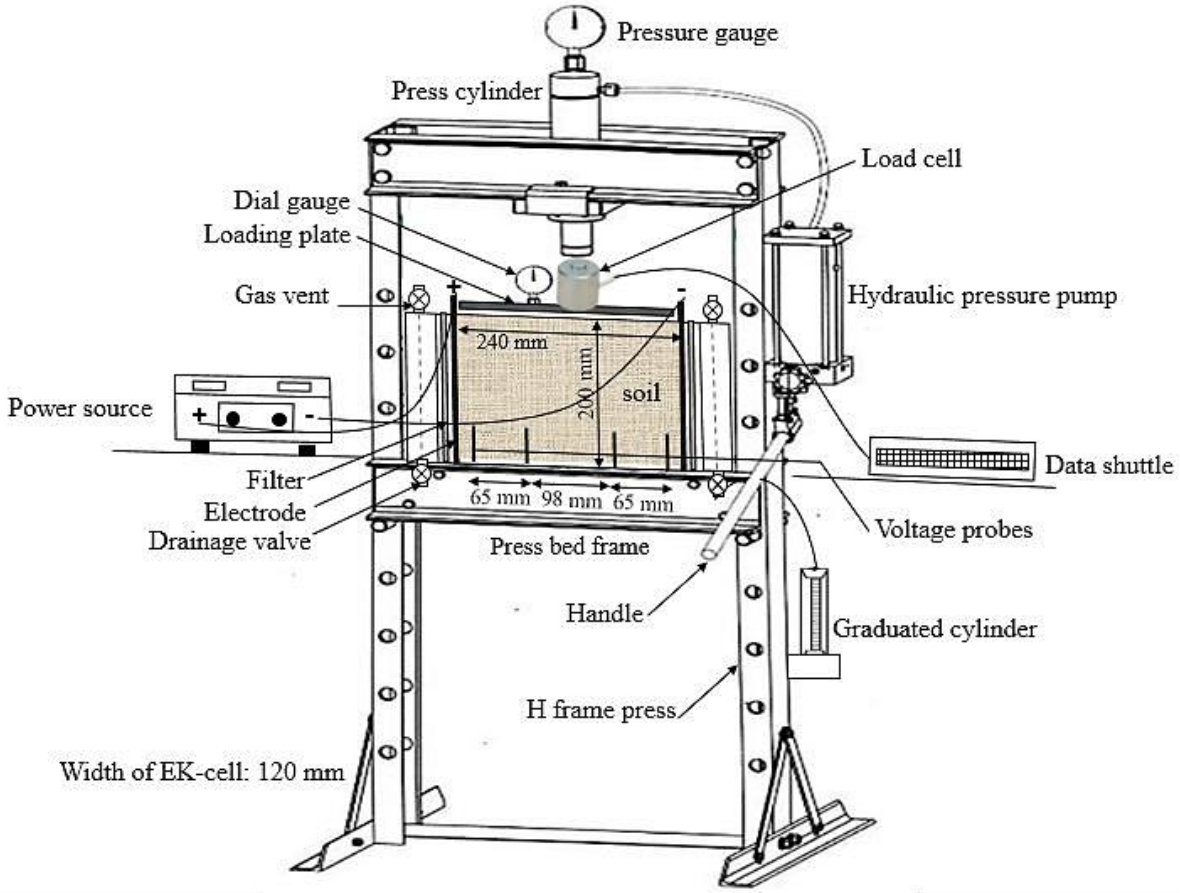

Fig. 5. Sketch of the experimental apparatus

2.4. Design of experiments

In this study, to assess the effectiveness of the electrokinetic process on soil consolidation and copper removal from water drained, experiments were divided into two groups of control and EKG experiments (Table 6). All the experiments were carried out with the same conditions, loading, drainage condition, and duration. The control experiment was conducted without the application of the electric field. However, electrokinetic geosynthetic experiments were carried out with the application of a constant voltage gradient of 1 ± 0.1 V/cm (Gray 1970) under the vertical pressure in the range of 7-113 kPa. The EKG experiments in three groups, including the C-EK (using carbon fiber), ES_1-EK (using carbon fiber plus electrospun nanofibers containing 1 wt% GNs), and ES_2-EK (using carbon fiber plus electrospun nanofibers containing 2 wt% GNs) were designed, as shown in Table 6.

Important parameters such as settlement, electric current, voltage, power consumption, drained water, and applied loads were recorded during the experiments at different time intervals, and copper concentration was measured at the end of the experiments. At the end of the experiments, the longitudinal distance between the anode and cathode electrodes was divided into 5 sections at a distance of 1, 6, 13, 19, and 24 cm from the anode. About 70 g of

soil sample was extracted from each section to determine the copper concentration according to the EPA 3050B method (EPA 1996).

To determine if the findings of experiments could be used, experiments were replicated three times in the same conditions. Statistical analyses, such as standard deviation, standard error, and independent samples t-test, were carried out by SPSS 26. The independent samples t-test compares the means of two independent groups to determine whether there is statistical evidence that the associated means are significantly different. If a p-value reported from a t-test is less than 0.05, that result is said to be statistically significant. If a p-value is greater than 0.05, the result is insignificant.

Table 6

Experiment conditions.

Experiment	Description	Electrodes	Applied loads (kPa)	Gradient voltage (V/cm)	Duration (h)
CT	Control test	-	7-113	-	60
C-EK	EKG experiment	Carbon fiber	7-113	1	60
ES_1-EK	EKG experiment	Electrospun fiber[a]	7-113	1	60
ES_2-EK	EKG experiment	Electrospun fiber[b]	7-113	1	60

a Electrospun nanofibers containing 1 wt% graphene nanoparticles
b Electrospun nanofibers containing 2 wt% graphene nanoparticles

3. Results

3.1. Fabrication of EKG electrodes

Although the optimal polymer concentration is chosen based on a trial-and-error method, 15 wt% PMMA (M_w=120 000) concentration was suggested by Khanlou et al. (2014) and Khanlou et al. (2015) to fabricate the smaller fiber diameter via electrospinning.

Electrospinning was initially performed by injecting a 15 wt% PMMA solution without adding nanofillers to the liquid feeding system. The fibers were discontinuous with a very short length and many beads (Fig. 6 (a)).

By increasing the polymer concentration to 18 wt%, the solution could form fibers, and the appearances of them changed from polymeric beads to continuous beaded fibers. Spherical-shaped beads also became spindle-shaped beads. However, fibers had wavy, irregular shapes (Fig. 6 (b)).

According to Gupta et al. (2005), the critical chain overlap concentration (c^*) of PMMA (at M_w of 120 000 g/mol) was about 3.4 wt%. Hence, by increasing the polymer concentration to 18 wt%, the ratio of the considered concentration (18 wt%) to the critical chain overlap concentration (3.4 wt%) obtained 5.3 in the semi-dilute entangled regime (c/c^*> 3), which provided better conditions for the electrospinning.

By adding graphite (in a 4 wt% concentration) to 18 wt% PMMA, the polymer solution's viscosity increased, and the appearance changed from beaded fibers to fibers with a cylindrical cross-section (Fig. 6 (c)). Graphite also improved the structure of the fibers; however, the fabricated fibers were fragmented.

The addition of graphene nanoparticles with concentrations of 1 and 2 wt% to 18 wt% PMMA solution changed the orientation of the fibers, removed twist of fibers, and fabricated straight fibers, which can be caused by the high repulsion between the fibers due to surface charge accumulation. Fiber repulsion helped to parallelize the fibers to reduce energy levels and increase more stability. Beads in the fibers obtained from the solution containing 18 wt% PMMA with 1 wt% GNs became more elongated due to the increase in viscosity, and uniform nanofibers were fabricated with the lowest number of beads (Fig. 6 (d)). By increasing the concentration of GNs to 2 wt%, continuous bead-free fibers were formed (Fig. 6 (e)).

Increasing the GNs concentration from 2 to 3 wt% and decreasing PMMA concentration from 18 to 13 wt% caused low viscosity of the solution. On the other hand, the accumulation of GNs among electrospun fibers was due to their high concentration. With the low concentration of polymer solution, Fibers were defective with a large number of beads (Fig. 6 (f)).

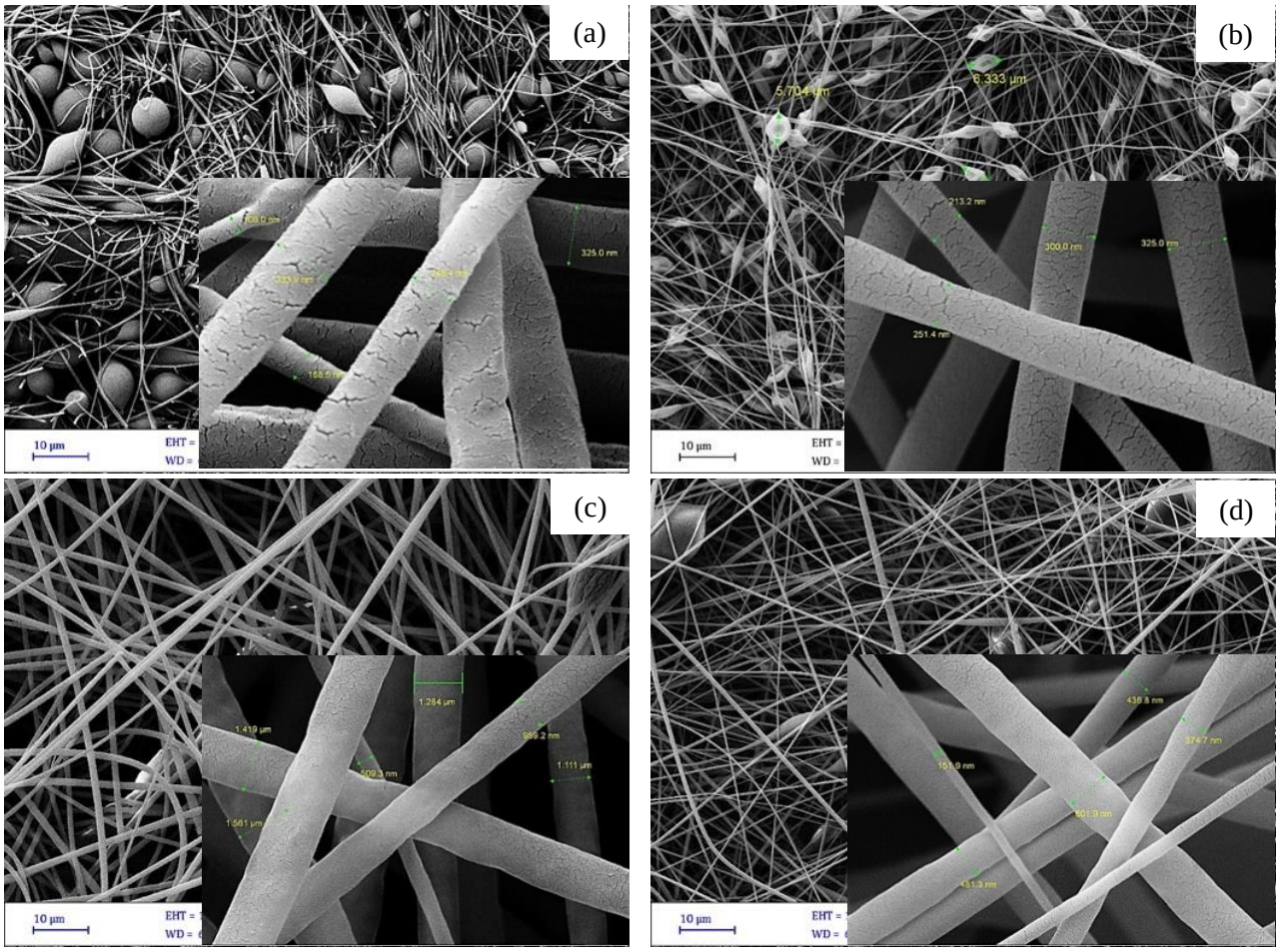

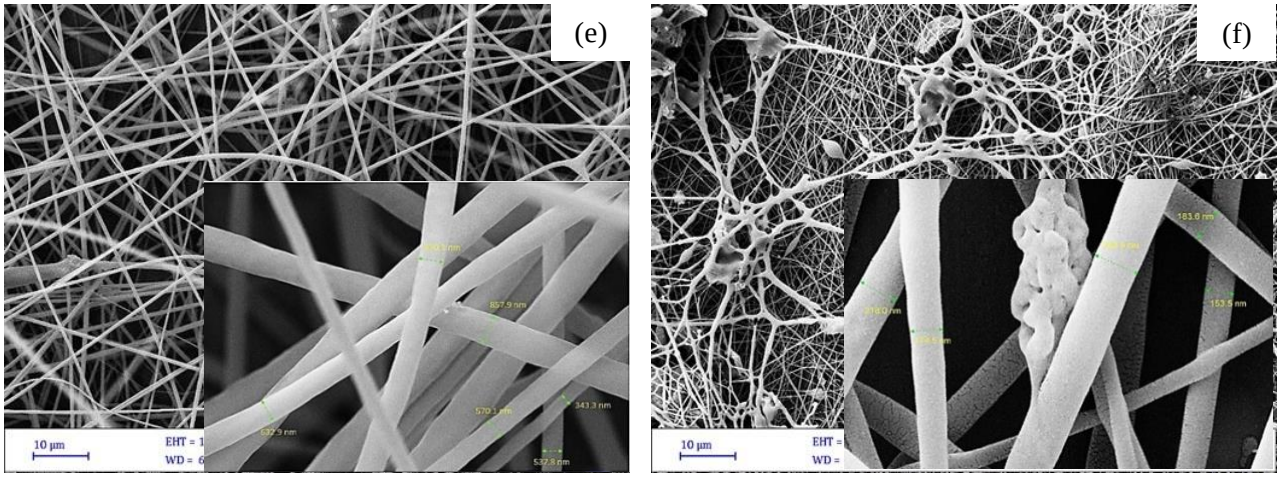

Fig. 6. Field emission scanning electron microscopy of fibers electrospun at different wt% of PMMA and fillers (a) 15 wt% PMMA, (b) 18 wt% PMMA, (c) 18 wt% PMMA with 4 wt% Graphite, (d) 18 wt% PMMA with 1 wt% GNs, (e) 18 wt% PMMA with 2 wt% GNs, (f) 13 wt% PMMA with 3 wt% GNs

3.2. Consolidation settlement

The cumulative settlement, followed by a decrease in the height of the soil sample under various loading (in the control experiment) and addition of an electric field (in EKG experiments), was shown in Fig. 7. The dash-dotted line in Fig. 7 shows the initial height of the soil sample, which was 190 mm.

The settlement shape in conventional consolidation (in the control experiment) was almost linear. In other words, the mean settlement was performed in one step and with a constant slope, as vertical pressure increased from 7 to 113 kPa.

According to Wang et al. (2018), the shape of the settlement in EKG experiments was non-linear (Fig. 7), and the application of the electric field, despite loading, increased settlement during EKG experiments. Therefore, settlement differences between control and EKG experiments were because of the electrokinetic process that occurred in the system (Micic et al. 2001). In other words, consolidation was performed by electroosmosis (Liu et al. 2014), which accelerated soil settlement.

The cumulative settlement in EKG experiments can be divided into three stages (Wu et al. 2020). In the first stage, the settlement occurred at the highest rate due to the application of the electric field. This stage was 40% of the total experiment duration and was performed in the pressure range 0-29 kPa. Increasing the pressure up to 60 kPa initiated the second stage of the settlement. At this stage, the settlement rate decreased compared to the first stage, but the settlement values were still higher than the control experiment. The incidence of the non-linear trend at 80% of the total experiment duration (the first and second stages) indicated that the impact of the electrokinetic process was dominant over the impact of loading. After increasing the vertical pressure up to 113 kPa in the third stage, the settlement trend changed and became similar to the linear trend in the control experiment, implying that the impact of the

electrokinetic process decreased in the system and the impact of loading at the last 20% of the total experiment duration increased.

Because the electroosmosis process occurs in a short period of the experimental duration (Rittirong et al. 2008), the electro-osmotic consolidation settlement also occurs in a short and limited time, and it does not continue simultaneously with the conventional consolidation settlement. Hence, after 40% of the experiment duration (end of the first stage), 66% of the total settlement in EKG experiments was obtained. In comparison, only 39% of the total settlement, at the same time, was completed in the control experiment. On the other hand, the mean strain in EKG experiments was 1.8 times the strain in the control experiment at the same time.

On the other hand, the coefficient of consolidation (C_v) was calculated to determine the average degree of consolidation over the entire layer (U_{ave}). The C_v displays the rate of pore water pressure dissipation, and as it increases, the rate of pore water pressure dissipation increases as well (Zhang et al. 2020). The C_v was calculated in the experiments as follows: $1 \cdot 6 \times 10^{-7}$ m^2/s in the control experiment and $2 \cdot 4 \times 10^{-7}$, $2 \cdot 6 \times 10^{-7}$, and $2 \cdot 8 \times 10^{-7}$ m^2/s in the C-EK, ES_1-EK, and ES_2-EK, respectively. Therefore, the determined U_{ave} according to the C_v was 68% in the control experiment and 85% in the EKG experiments.

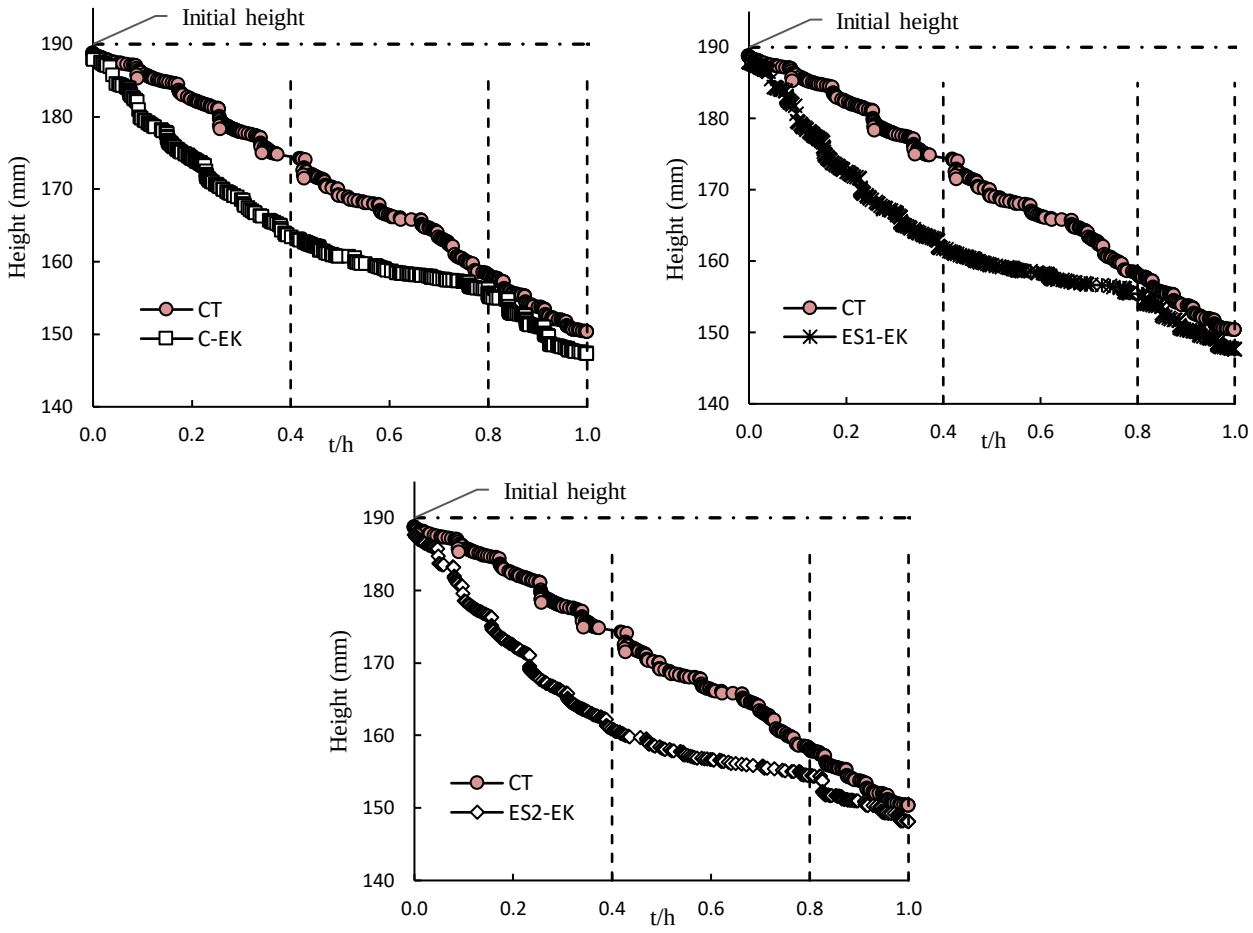

Fig. 7. The settlement versus time

3.3. Electric current and power consumption

Changes in the electric current versus time in the EKG experiments were shown in Fig. 8. In the C-EK, the electric current increased from 0.36 A to 0.38 A within the first 120 minutes of the experiment duration and then reached 0.1 A, as time went on. After the initial electric current fluctuations in ES_1-EK and ES_2-EK, the electric current reduced from 0.35 to 0.1 A.

The changes in electric current versus time had a declining trend during EKG experiments. According to Micic et al. (2003), the decrease in electric current versus time under a constant voltage gradient is typical in all electrokinetic systems, because the conduction of electric current in the system is affected by ions. Thus, the long-term reduction in electric current was due to dewatering, which led to less electrically conductive regions in the system (Bourgès-Gastaud et al. 2017).

There was no significant difference between the electric current values (Fig. 8) in EKG experiments. On the other hand, a sudden drop in electric current in C-EK, ES_2-EK, and ES_1-EK experiments occurred after 50%, 40%, and 30% of the total experiment duration, respectively, indicating an increase in soil electrical resistance at times mentioned.

Power consumption of electro-osmotic consolidation was calculated by multiplying the voltage between the two electrodes, the electric current, and the time in each step. Then, it was divided by the volume of soil in that time step to calculate the ratio of energy to soil volume. In Fig. 8, cumulative energy consumption versus time was also shown in addition to changes in electric current. As the experiments progressed, power consumption gradually increased from 2.8 to 31.8 kWh/m^3 in the C-EK, from 2.6 to 26.7 kWh/m^3 in the ES_1-EK, and from 2.5 to 27.9 kWh/m^3 in the ES_2-EK.

Power consumption, as a function of electric current, grows with an increase in electric current. The percentage increase in total power consumption in the C-EK was 19.3% compared to the ES_1-EK and 14.1% compared to the ES_2-EK. At the end of the electrokinetic process, the total power consumption in the ES_2-EK increased by 4.6% compared to the ES_1-EK.

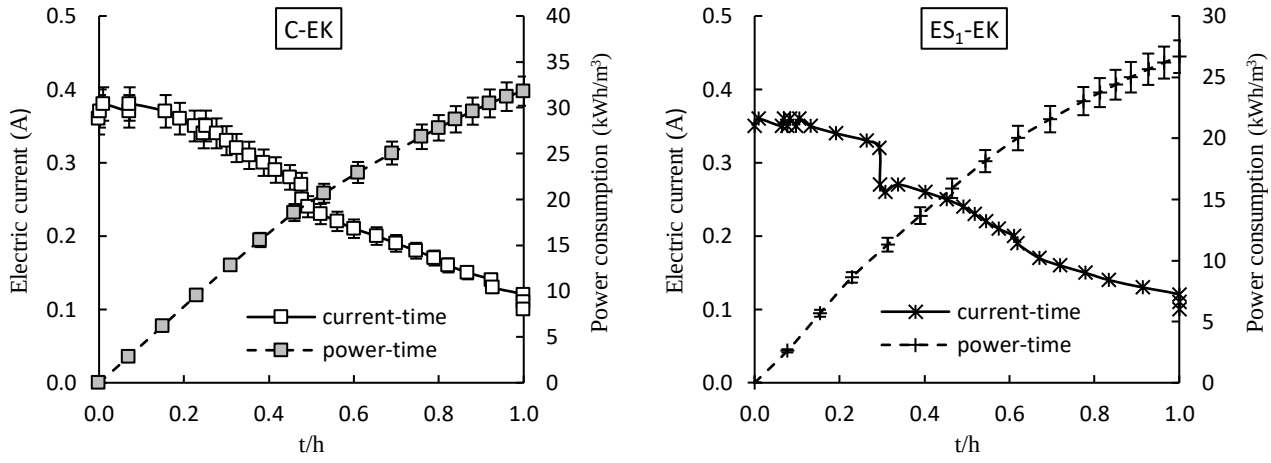

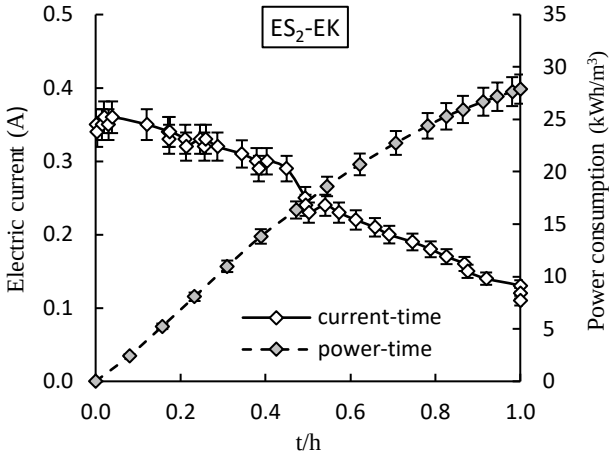

Fig. 8. Electric current and power consumption versus time

3.4. Remaining copper concentration in the soil

After the completion of experiments, the remaining copper concentration was determined at a distance between the anode and cathode by the acid digestion method (EPA 1996); the results were presented in Fig. 9 (a). The dash-doted line in Fig. 9 (a) shows the initial concentration of copper in the soil, which is 200 mg/kg. The decrease in copper concentration in the control experiment almost similarly occurred in all longitudinal sections, and it was due to pore water drainage in the conventional consolidation.

According to the remaining copper concentration at the end of EKG experiments, copper accumulation was observed in two sections. One of those was adjacent to the anode (at a normalized distance of 0.04 from the anode), and the other was in the middle distance between the two electrodes (at a normalized distance of 0.5 from the anode). The section adjacent to the anode contained the highest copper concentration compared to the middle section. This is due to the accumulation of anionic metal complexes (Behrouzinia et al. 2021). Following the impossibility of moving the copper due to the weak electric field, copper was accumulated in the middle section (Reddy and Chinthamreddy 2004).

In other sections (at a normalized distance of 0.25, 0.75, and 0.096 from the anode), the remaining copper concentration in EKG experiments decreased compared to the control experiment. The reasons for that occurrence were the formation of anionic metal complexes and their movement towards the anode at a normalized distance of 0.25 from the anode and the movement of Cu^{2+} towards the cathode at a normalized distance of 0.75 from the anode. Because of the time delay in water drainage from the system, copper concentration at a normalized distance of 0.96 from the anode was slightly higher than in the previous section.

The final copper concentration in the water drained from the cathode was shown in Fig. 9(b). As expected, the drained water in the control experiment contained the highest copper concentration. The lowest copper concentration was obtained in ES_2-EK and ES_1-EK, respectively. The remaining copper concentration of drained water in the control experiment

was 6.7, 13.1, and 37.3 times the remaining copper concentration in the C-EK, ES_1-EK, and ES_2-EK, respectively. It implied the effect of the electroosmosis process and the application of fabricated geosynthetic electrodes.

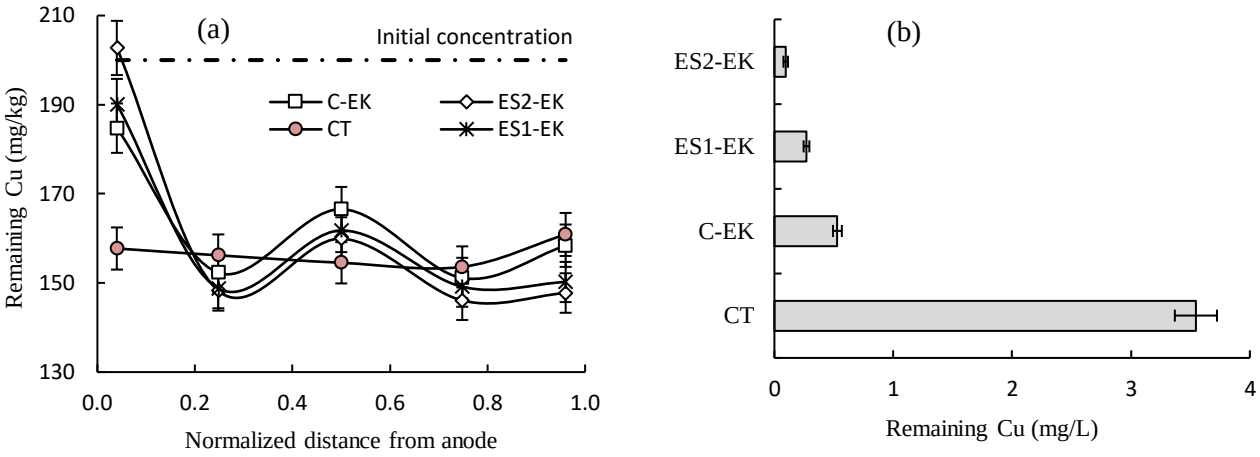

Fig. 9. Remaining copper concentration (a) in the soil, (b) in drained water

4. Discussion

4.1. Evaluation of EKG electrodes

In this section, the diameter distribution of electrospun fibers, depending on the solution properties, was investigated by the box and whisker diagram (Fig. 10). The average diameter of fibers obtained from 18 wt% PMMA was 343 ± 31 nm. Moreover, the nanofibers had the narrowest diameter distribution among others, which implied that the fiber diameters were uniform. The fibers obtained from the solution containing 18 wt% PMMA with 4 wt% graphite with an average diameter of 1234 ± 111 nm had the widest diameter distribution among others. Besides, the diameter of fibers fabricated by 4 wt% graphite had exceeded the final diameter of the nanofibers (1000 nm) expressed by Matsumoto and Tanioka (2011); Tanioka and Takahashi (2016). The average diameters of fibers obtained from 18 wt% PMMA solution containing 1 and 2 wt% GNs were 404 ± 36 and 690 ± 62, respectively. The diameter distribution of the solution with 2 wt% GNs, which caused more non-uniformity in fiber diameter, was wider than that of the solution with 1 wt% GNs. By reducing the polymer concentration to 13 wt% and increasing the GNs concentration to 3 wt%, the average diameter of electrospun fibers reached a minimum value of 168 ± 15 nm. According to Lamastra et al. (2012), the diameter of fibers depends on the electrical conductivity and viscosity of the solution, and fibers with very small diameters can be obtained from polymer solution with low viscosity and high electrical conductivity.

According to the results, 18 wt% PMMA solutions containing 1 and 2 wt% GNs were selected as suitable polymer solutions to fabricate nanofibrous layers on carbon fibers. GNs in

that concentration had significant impacts on beads removing and fiber structure improving.

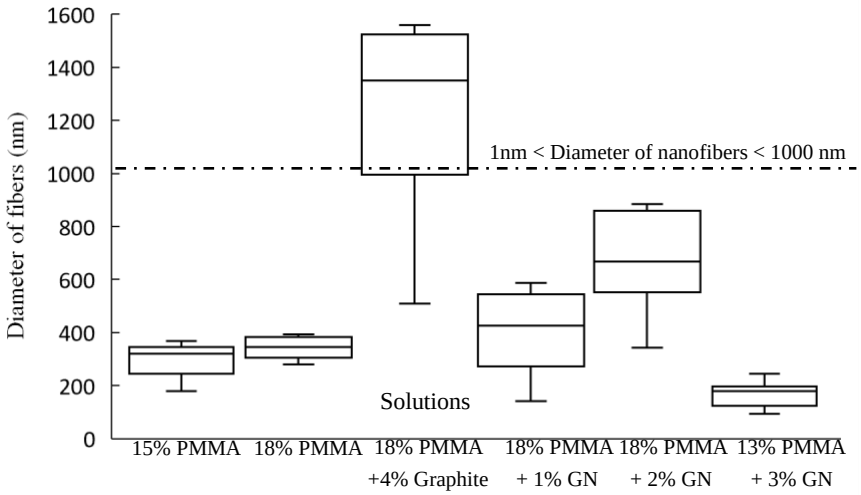

Fig. 10. Diameter distribution of electrospun fibers

4.2. Evaluation of consolidation settlement

To compare the means between two experiments and determine if there is a significant difference between them, independent samples t-test was conducted (Table 7). According to Table 7, There was a significant difference ($p < 0.05$) at the 95% confidence level between the settlement results obtained from EKG experiments and the control experiment. Moreover, the results of the t-test indicated that there was no significant difference at the 95% confidence level among the results of ES_1-EK, ES_2-EK, and C-EK. Therefore, EKG electrodes fabricated based on the electrospinning technique did not significantly change the settlement values. In other words, attaching the composite nanofibers onto the carbon fiber did not have a negative effect on the electric current intensity and electro-osmotic consolidation. And, it led to performing settlement in accordance with the pattern implemented by the application of carbon fibers as electrodes. Furthermore, there was no significant difference at the 95% confidence level between the results of ES_1-EK and ES_2-EK (Table 7). Hence, increasing the concentration of GNs from 1 to 2 wt% did not cause a significant difference in settlements.

Table 7

P-values of independent samples t-test in settlements.

Experiment	CT				
C-EK	2.56 E-15	Experiment	C-EK		
ES_1-EK	7.13 E-10	ES_1-EK	0.126	Experiment	ES_1-EK
ES_2-EK	4.53 E-24	ES_2-EK	0.647	ES_2-EK	0.292
	$p < 0.05$		$p > 0.05$		$p > 0.05$

Following conventional consolidation in the control experiment and electro-osmotic consolidation in the EKG experiments, the void ratio was calculated in all stages of consolidation. Fig. 11 displays the void ratio versus effective stress applied during experiments. As expected, the increase in effective stress caused the decrease in the void ratio. The compression index (C_c) was defined as the slope of the line (Eq. (1)) in the e-log σ coordinate system. In the control experiment, C_c based on the slope of the trendline equation was 0.43. On the other hand, C_c was 0.35 in the C-EK and 0.37 in the ES_1-EK and ES_2-EK.

$$e = e_\circ - C_c \log(\sigma'/\sigma_\circ) \tag{1}$$

where $e_\circ$ is the initial void ratio; C_c is the compression index; $\sigma_\circ$ is the initial effective stress.

In EKG experiments, the coefficient of electro-osmotic conductivity was calculated based on the equation expressed by Mitchell and Soga (2005) (Eq. (2)); it was shown versus void ratio in Fig. 11.

$$K_e = \frac{Q}{A \cdot i_e} \tag{2}$$

where K_e is the coefficient of electro-osmotic conductivity in m^2/V.sec; Q is the volume flow rate in m^3/s; A is the cross-sectional area in m^2; i_e is the electrical potential gradient in V/m.

According to Fig. 11, K_e in EKG experiments ranged between 1×10^{-9} and 1×10^{-8} m^2/V.sec, as expressed by Martin et al. (2019). As the void ratio decreased, the K_e decreased (Badv and Mohammadzadeh 2015). Based on the trendline equation proposed in Fig. 11, variations of soil compressibility and electroosmosis conductivity were non-linear in electro-osmotic consolidation, as well (Wu et al. 2017).

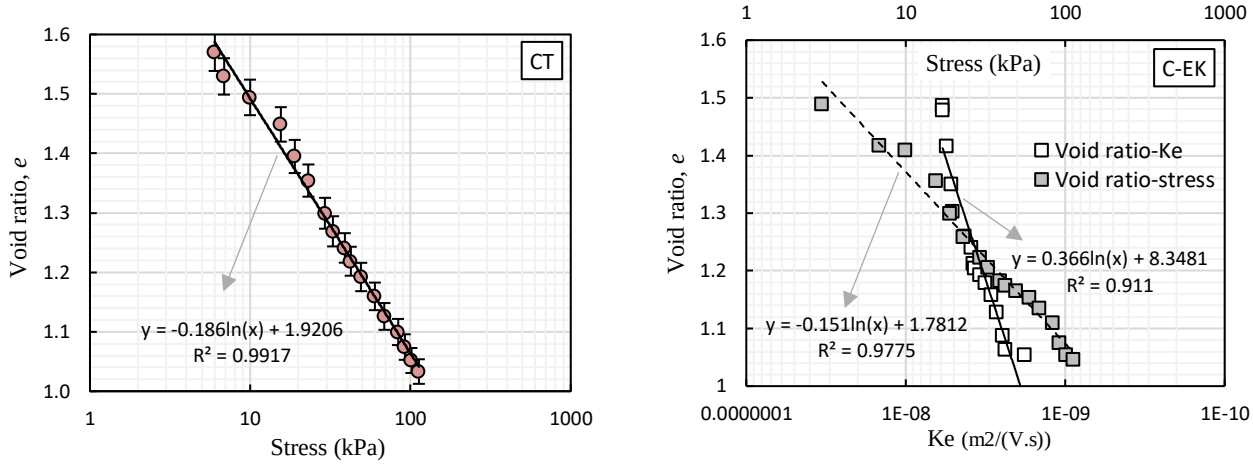

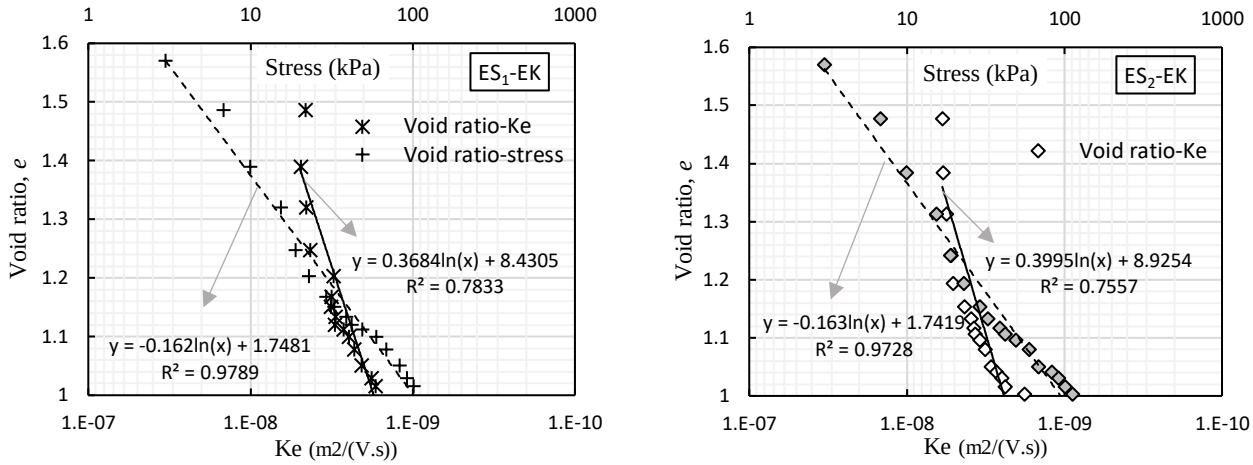

Fig. 11. Relationships between void ratio and effective stress; void ratio and electro-osmotic conductivity

4.3. Variations of electric current and power consumption

Fig. 8 showed the small fluctuations of electric current in the experiments with geosynthetic electrodes, which was very important about applying a uniform electric field. In other words, EKG electrodes had a small variation in electric current versus time (Xiao et al. 2021).

As expressed by Zhang and Hu (2019), the electric current depends on the number of ionic species in the pore water, so that at high initial ion concentration, the electric current increases, and with the decrease in ion concentration, due to physicochemical changes, electromigration, and electro-osmotic flow during the progress of the experiments, the electric current decreases. Thus, the continuous declining trend of electric current in Fig. 8 had been because of the gradual removal of soluble ions as a transmitting agent.

To evaluate the effectiveness of geosynthetic electrokinetic, the relationship between total energy consumption per unit volume of soil and water content at the end of the experiments was shown in Fig. 12 (a). Water content in Fig. 12 (a) was the average value of soil water content obtained from 5 consecutive sections between the anode and cathode after disconnecting the power supply.

The decrease in soil water content, due to conventional and electro-osmotic consolidation, was calculated by Eq. (3) presented by Micic et al. (2001). In Eq. (3), Δw is the decrease in water content, whereas $\Delta w_{(l)}$ exhibits the decrease in water content due to loading, and $\Delta w_{(EK+l)}$ shows the decrease in water content due to both electro-osmotic and loading impacts. $\Delta w_{(EK)}$ displays a decrease in water content under the impact of the electrokinetic process that is calculated by the difference of those values.

$$\Delta w_{(EK)} = \Delta w_{(EK+l)} - \Delta w_{(l)} \quad (3)$$

Similar to the β parameter used as energy utilization efficiency in electrokinetic remediation (Behrouzinia et al. 2021), the λ parameter was introduced as the energy utilization efficiency in electro-osmotic consolidation (Fig. 12 (b)). To calculate λ, the values of water content were used instead of removal efficiency (Eq. (4)).

$$\lambda = \frac{\theta}{W} \tag{4}$$

where λ is the energy utilization efficiency; θ is the water content in %; W is the total power consumption in Wh.

High values of λ mean high energy utilization efficiency, i.e., with less energy consumption, more water content is removed from the soil. λ had the highest values in ES_1-EK and ES_2-EK, respectively, and the lowest values in C-EK.

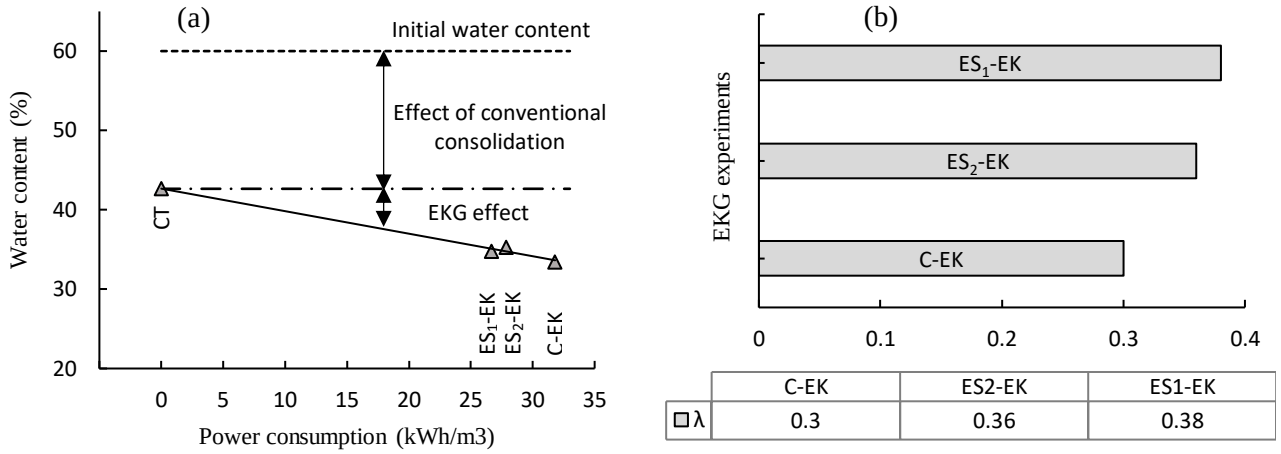

Fig. 12. (a) Variations of water content with power consumption, (b) Energy utilization efficiency

4.4. The removal efficiency of copper

Using the copper concentration of water drained within the cathode (Fig. 9 (b)), the copper removal efficiency of the geosynthetic electrode was calculated, as shown in Fig. 13. The removal efficiency of copper was determined based on the remaining copper concentration of water drained from EKG experiments to the control experiment. Therefore, the copper removal efficiency of the control experiment was zero.

The highest copper removal efficiencies were obtained in ES_2-EK (97%) and ES_1-EK (92%), respectively. The lowest efficiency of copper removal was obtained in the C-EK (85%) due to performing the reduction reaction at the cathode and the capability of carbon fibers to remove copper, as well. The difference in the efficiency showed the high capability of the composite

nanofibers attached to the carbon fiber to remove the copper from water drained within the cathode, which is affected by the high specific surface area of the electrospun nanofibers.

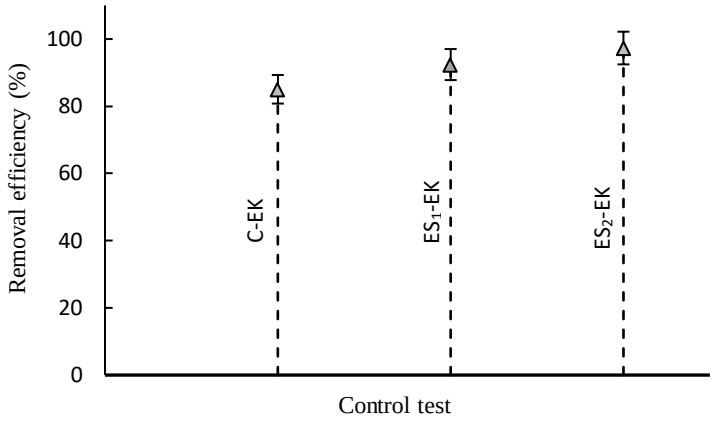

Fig. 13. Copper removal efficiency in drained water

5. Conclusions

In this study, a new EKG electrode was fabricated by attaching electrospun composite nanofibers to a carbon fiber substrate with an electrical resistance of $1 \cdot 7 \times 10^{-5}\ \Omega \cdot \mathrm{m}$, and its effectiveness was evaluated in electro-osmotic consolidation of soil and copper removal from drained water. ES_1-EK, ES_2-EK (using electrodes containing electrospun nanofibers with 1 and 2 wt% GNs, respectively), and C-EK (using carbon fiber electrodes) were categorized as EKG experiments, and their results were analyzed in comparison with the control experiment.

- Carbon fibers were efficient as the substrate structure of electrodes for different reasons, oxidation resistance (unlike metal electrodes), high electrical conductivity (100 times more than the recommended electrical conductivity), the possibility of drainage within the fiber structure, effective contact surface with the soil profile, and a suitable and flexible structure for electrospinning.
- EKG electrodes fabricated based on electrospinning technique were effective as a drainage channel in copper removal and led to removal efficiencies more than 90%. Moreover, these electrodes accelerated the consolidation. The mean strain in EKG experiments was 1.8 times the strain in the control experiment.
- The power consumption in the C-EK was 16.6% higher than ES_1-EK and ES_2-EK. On the other hand, the energy utilization efficiency had the highest values in ES_1-EK (0.38) and ES_2-EK (0.36), respectively, and the lowest value in C-EK (0.3). Higher utilization efficiency indicated that more water content could be removed by less energy consumption.
- As the cause of high energy consumption is affected by two factors: corrosion of the electrodes and the strategy of applying the electric field, in addition to suppressing the

electrode corrosion in this research, the copper removal capability was attached to the structure by fabricating a new geosynthetic electrode. However, in future research, it is possible to reduce energy consumption and make the process economical by applying current intermittence instead of continuous DC. On the other hand, by changing the linear arrangement of the electrodes, the accumulation of copper in the middle of the model can be reduced, and its impact on the metal distribution can be evaluated.

Acknowledgements

The authors wish to express their appreciation to the Iranian Agricultural Engineering Research Institute (IAERI) and Urmia Univerisity for providing the facilities required to carry out the research.

References

Ahmad, K.A.K., Kassim, K.A.K.K.A. and TahaÂ, M.R.T.M.R., 2006. Electroosmotic flows and electromigrations during electrokinetic processing of tropical residual soil. *Malaysian Journal of Civil Engineering*, *18*(2).

Altin, A. and Degirmenci, M., 2005. Lead (II) removal from natural soils by enhanced electrokinetic remediation. *Science of the Total Environment*, *337*(1-3), pp.1-10.

Azhar, A.T.S., Azim, M.A.M., Syakeera, N.N., Jefferson, I.F. and Rogers, C.D.F., 2017. Application of Electrokinetic Stabilisation (EKS) Method for Soft Soil: A Review. In *IOP Conference Series: Materials Science and Engineering* (Vol. 226, No. 1, p. 012075). IOP Publishing.

Azhar, A.T.S., Jefferson, I., Madun, A., Abidin, M.H.Z. and Rogers, C.D.F., 2018, April. Electrokinetic stabilisation method of soft clay in pure system using electrokinetic geosynthetic electrode. In *Journal of Physics: Conference Series* (Vol. 995, No. 1, p. 012109). IOP Publishing.

Badv, K. and Mohammadzadeh, K., 2015. Laboratory assessment of the electro-osmotic consolidation technique for Urmia lake sediments. *Iranian Journal of Science and Technology Transactions of Civil Engineering*, 39(C2+), pp.485-496.

Ballabio, C., Panagos, P., Lugato, E., Huang, J.H., Orgiazzi, A., Jones, A., Fernández-Ugalde, O., Borrelli, P. and Montanarella, L., 2018. Copper distribution in European topsoils: An assessment based on LUCAS soil survey. *Science of The Total Environment*, 636, pp.282-298.

Bayat, O., Kilic, O., Bayat, B., Anil, M., Akarsu, H. and Poole, C., 2006. Electrokinetic dewatering of Turkish glass sand plant tailings. *Water research*, *40*(1), pp.61-66.

Behrouzinia, S., Ahmadi, H., Abbasi, N. and Javadi, A.A., 2021. Insights into enhanced electrokinetic remediation of copper-contaminated soil using a novel conductive membrane based on nanoparticles. *Environmental Geochemistry and Health*, pp.1-18.

Bergado, D.T., Sasanakul, I. and Horpibulsuk, S., 2003. Electro-osmotic consolidation of soft Bangkok clay using copper and carbon electrodes with PVD. *Geotechnical testing journal*, *26*(3), pp.277-288.

Bourgès-Gastaud, S., Dolez, P., Blond, E. and Touze-Foltz, N., 2017. Dewatering of oil sands tailings with an electrokinetic geocomposite. *Minerals Engineering*, *100*, pp.177-186.

Bourgès-Gastaud, S., Stoltz, G., Dolez, P., Blond, É. and Touze-Foltz, N., 2015. Laboratory device to characterize electrokinetic geocomposites for fluid fine tailings dewatering. *Canadian Geotechnical Journal*, *52*(4), pp.505-514.

Burnotte, F., Lefebvre, G. and Grondin, G., 2004. A case record of electroosmotic consolidation of soft clay with improved soil electrode contact. *Canadian Geotechnical Journal*, *41*(6), pp.1038-1053.

Cai, Z., Sun, Y., Deng, Y., Zheng, X., Sun, S., Romantschuk, M. and Sinkkonen, A., 2021. In situ electrokinetic (EK) remediation of the total and plant available cadmium (Cd) in paddy agricultural soil using low voltage gradients at pilot and full scales. *Science of The Total Environment*, *785*, p.147277.

Cao, B., Wang, R., Zhang, W., Wu, H. and Wang, D., 2019. Carbon-based materials reinforced waste activated sludge electro-dewatering for synchronous fuel treatment. *Water research*, *149*, pp.533-542.

Cao, B., Zhang, T., Zhang, W. and Wang, D., 2020. Enhanced technology based for sewage sludge deep dewatering: A critical review. *Water Research*, p.116650.

Cappello, S., Viggi, C.C., Yakimov, M., Rossetti, S., Matturro, B., Molina, L., Segura, A., Marqués, S., Yuste, L., Sevilla, E. and Rojo, F., 2019. Combining electrokinetic transport and bioremediation for enhanced removal of crude oil from contaminated marine sediments: Results of a long-term, mesocosm-scale experiment. *Water research*, *157*, pp.381-395.

Chen, J.L., Yang, S.F., Wu, C.C. and Ton, S., 2011. Effect of ammonia as a complexing agent on electrokinetic remediation of copper-contaminated soil. *Separation and purification technology*, 79(2), pp.157-163.

Chew, S.H., Karunaratne, G.P., Kuma, V.M., Lim, L.H., Toh, M.L. and Hee, A.M., 2004. A field trial for soft clay consolidation using electric vertical drains. *Geotextiles and Geomembranes*, *22*(1-2), pp.17-35.

Chien, S.C., Ou, C.Y. and Wang, M.K., 2009. Injection of saline solutions to improve the electro-osmotic pressure and consolidation of foundation soil. *Applied clay science*, 44(3-4), pp.218-224.

Chowdhury, A.I., Gerhard, J.I., Reynolds, D., Sleep, B.E. and O'Carroll, D.M., 2017. Electrokinetic-enhanced permanganate delivery and remediation of contaminated low permeability porous media. *Water research*, *113*, pp.215-222.

Citeau, M., Larue, O. and Vorobiev, E., 2011. Influence of salt, pH and polyelectrolyte on the pressure electro-dewatering of sewage sludge. *Water Research*, *45*(6), pp.2167-2180.

Czinnerová, M., Vološčuková, O., Marková, K., Ševců, A., Černík, M. and Nosek, J., 2020. Combining nanoscale zero-valent iron with electrokinetic treatment for remediation of chlorinated ethenes and promoting biodegradation: a long-term field study. *Water research*, *175*, p.115692.

Deng, A. and Zhou, Y., 2016. Modeling electroosmosis and surcharge preloading consolidation. II: Validation and simulation results. *Journal of Geotechnical and Geoenvironmental Engineering*, *142*(4), p.04015094.

Dos Santos, E.V., Ferro, S. and Vocciante, M., 2020. Electrokinetic remediation. *The Handbook of Environmental Remediation: Classic and Modern Techniques*, p.121.

EPA, E.,1996. Method 3050B-Acid digestion of sediments, sludges and soils. Test Methods for Evaluating Solid Wastes: Physical/Chemical Methods. EPA SW-846, 1, 3050B-1.

Eriksson, F. and Gemvik, L., 2014. Electro-Osmotic Treatment of Soil: A laboratory investigation of three Swedish clays.

Flora, A., Gargano, S., Lirer, S. and Mele, L., 2017. Experimental evidences of the strengthening of dredged sediments by electroosmotic consolidation. *Geotechnical and Geological Engineering*, *35*(6), pp.2879-2890.

Fourie, A.B. and Jones, C.J.F.P., 2010. Improved estimates of power consumption during dewatering of mine tailings using electrokinetic geosynthetics (EKGs). *Geotextiles and Geomembranes*, *28*(2), pp.181-190.

Fourie, A.B., Johns, D.G. and Jones, C.F., 2007. Dewatering of mine tailings using electrokinetic geosynthetics. *Canadian geotechnical journal*, *44*(2), pp.160-172.

Fu, H., Fang, Z., Wang, J., Chai, J., Cai, Y., Geng, X., Jin, J. and Jin, F., 2018. Experimental comparison of electroosmotic consolidation of wenzhou dredged clay sediment using intermittent current and polarity reversal. *Marine Georesources & Geotechnology*, *36*(1), pp.131-138.

Fu, H., Yuan, L., Wang, J., Cai, Y., Hu, X. and Geng, X., 2019. Influence of high voltage gradients on electrokinetic dewatering for Wenzhou clay slurry improvement. *Soil Mechanics and Foundation Engineering*, *55*(6), pp.400-407.

Fu, H.T., Cai, Y.Q., Wang, J. and Wang, P., 2017. Experimental study on the combined application of vacuum preloading–variable-spacing electro-osmosis to soft ground improvement. *Geosynthetics International*, *24*(1), pp.72-81.

Gargano, S., Lirer, S. and Flora, A., 2019. Analysis of the coupled electro-osmotic and mechanical consolidation in clayey soils. *Proceedings of the Institution of Civil Engineers-Ground Improvement*, *172*(3), pp.146-157.

Ghobadi, R., Altaee, A., Zhou, J.L., Karbassiyazdi, E. and Ganbat, N., 2021. Effective remediation of heavy metals in contaminated soil by electrokinetic technology incorporating reactive filter media. *Science of The Total Environment*, *794*, p.148668.

Gray, D.H., 1970. Electrochemical hardening of clay soils. *Geotechnique*, *20*(1), pp.81-93.

Guo, X., Wang, Y. and Wang, D., 2017. Permanganate/bisulfite (PM/BS) conditioning–horizontal electro-dewatering (HED) of activated sludge: effect of reactive Mn (III) species. *Water research*, *124*, pp.584-594.

Gupta, P., Elkins, C., Long, T.E. and Wilkes, G.L., 2005. Electrospinning of linear homopolymers of poly (methyl methacrylate): exploring relationships between fiber formation, viscosity, molecular weight and concentration in a good solvent. *Polymer*, 46(13), pp.4799-4810.

Hamir, R.B., Jones, C.J.F.P. and Clarke, B.G., 2001. Electrically conductive geosynthetics for consolidation and reinforced soil. *Geotextiles and Geomembranes*, 19(8), pp.455-482.

Hu, J., Li, X., Zhang, D., Wang, J., Hu, X. and Cai, Y., 2020. Experimental Study on the Effect of Additives on Drainage Consolidation in Vacuum Preloading Combined with Electroosmosis. *KSCE Journal of Civil Engineering*, *24*(9), pp.2599-2609.

Hu, L., Wu, H. and Wen, Q.B., 2013. Electro-osmotic consolidation: Laboratory tests and numerical simulation. In *The 18th International Conference on Soil Mechanics and Geotechnical Engineering, Paris* (pp. 231-234).

Hu, L., Zhang, L. and Wu, H., 2019. Experimental study of the effects of soil pH and ionic species on the electro-osmotic consolidation of kaolin. *Journal of hazardous materials*, *368*, pp.885-893.

Jones, C.J., Lamont-Black, J., Glendinning, S., White, C. and Alder, D., 2014, June. The environmental sustainability of electrokinetic geosynthetic strengthened slopes. In *Proceedings of the Institution of Civil Engineers-Engineering Sustainability* (Vol. 167, No. 3, pp. 95-107). Thomas Telford Ltd.

Kalumba, D., Glendinning, S., Rogers, C.D.F., Tyrer, M. and Boardman, D.I., 2009. Dewatering of tunneling slurry waste using electrokinetic geosynthetics. *Journal of Environmental Engineering*, *135*(11), pp.1227-1236.

Kaniraj, S.R. and Yee, J.H.S., 2011. Electro-osmotic consolidation experiments on an organic soil. *Geotechnical and Geological Engineering*, *29*(4), pp.505-518.

Kaniraj, S.R., 2014. Soft soil improvement by electroosmotic consolidation. *International Journal of Integrated Engineering*, *6*(2).

Kaniraj, S.R., Huong, H.L. and Yee, J.H.S., 2011. Electro-osmotic consolidation studies on peat and clayey silt using electric vertical drain. *Geotechnical and Geological Engineering*, *29*(3), pp.277-295.

Karunaratne, G.P., Jong, H.K. and Chew, S.H., 2004. New electrically conductive geosynthetics for soft clay consolidation. In Proceeding of the 3rd Asian Regional Conference on Geo-synthetics (pp. 277-284).

Khanlou, H.M., Chin Ang, B., Talebian, S., Muhammad Afifi, A. and Andriyana, A., 2015. Electrospinning of polymethyl methacrylate nanofibers: optimization of processing parameters using the Taguchi design of experiments. *Textile Research Journal*, 85(4), pp.356-368.

Khanlou, H.M., Sadollah, A., Ang, B.C., Kim, J.H., Talebian, S. and Ghadimi, A., 2014. Prediction and optimization of electrospinning parameters for polymethyl methacrylate nanofiber fabrication using response surface methodology and artificial neural networks. *Neural Computing and Applications*, 25(3-4), pp.767-777.

Lamastra, F.R., Puglia, D., Monti, M., Vella, A., Peponi, L., Kenny, J.M. and Nanni, F., 2012. Poly (ε-caprolactone) reinforced with fibres of poly (methyl methacrylate) loaded with multiwall carbon nanotubes or graphene nanoplatelets. *Chemical Engineering Journal*, 195, pp.140-148.

Lamont-Black, J., Hall, J.A., Glendinning, S., White, C.P. and Jones, C.J., 2012. Stabilization of a railway embankment using electrokinetic geosynthetics. *Geological Society, London, Engineering Geology Special Publications*, *26*(1), pp.125-139.

Lamont-Black, J., Jones, C.J. and White, C., 2015. Electrokinetic geosynthetic dewatering of nuclear contaminated waste. *Geotextiles and Geomembranes*, *43*(4), pp.359-362.

Lee, J.K., Shang, J.Q. and Xu, Y., 2016. Electrokinetic dewatering of mine tailings using DSA electrodes. *Int. J. Electrochem. Sci*, *11*(5), pp.4149-4160.

Li, H., Wang, Y. and Zheng, H., 2018. Variations of moisture and organics in activated sludge during $Fe^0/S_2O_8^{2-}$ conditioning–horizontal electro-dewatering process. *Water research*, *129*, pp.83-93.

Li, L., Jiang, Z., Li, M., Li, R. and Fang, T., 2014. Hierarchically structured PMMA fibers fabricated by electrospinning. *Rsc Advances*, 4(95), pp.52973-52985.

Ling, J., Li, X., Qian, J. and Li, X., 2021. Performance comparison of different electrode materials for electro-osmosis treatment on subgrade soil. *Construction and Building Materials*, *271*, p.121590.

Liu, H.L., Cui, Y.L., Shen, Y. and Ding, X.M., 2014. A new method of combination of electroosmosis, vacuum and surcharge preloading for soft ground improvement. *China Ocean Engineering*, 28(4), pp.511-528.

Lu, P. and Ding, B., 2008. Applications of electrospun fibers. *Recent patents on nanotechnology*, 2(3), pp.169-182.

Mahmoud, A., Hoadley, A.F., Citeau, M., Sorbet, J.M., Olivier, G., Vaxelaire, J. and Olivier, J., 2018. A comparative study of electro-dewatering process performance for activated and digested wastewater sludge. *Water research*, *129*, pp.66-82.

Mahmoud, A., Hoadley, A.F., Conrardy, J.B., Olivier, J. and Vaxelaire, J., 2016. Influence of process operating parameters on dryness level and energy saving during wastewater sludge electro-dewatering. *Water research*, *103*, pp.109-123.

Mahmoud, A., Olivier, J., Vaxelaire, J. and Hoadley, A.F., 2010. Electrical field: A historical review of its application and contributions in wastewater sludge dewatering. *Water research*, *44*(8), pp.2381-2407.

Mahmoud, A., Olivier, J., Vaxelaire, J. and Hoadley, A.F., 2011. Electro-dewatering of wastewater sludge: influence of the operating conditions and their interactions effects. *Water Research*, *45*(9), pp.2795-2810.

Malekzadeh, M. and Sivakugan, N., 2021, April. Laboratory evaluation of electrokinetic dewatering of dredged marine sediment as an option for climate change adaption. In *IOP Conference Series: Earth and Environmental Science* (Vol. 710, No. 1, p. 012030). IOP Publishing.

Malekzadeh, M., Lovisa, J. and Sivakugan, N., 2016. An overview of electrokinetic consolidation of soils. *Geotechnical and Geological Engineering*, *34*(3), pp.759-776.

Martin, L., Alizadeh, V. and Meegoda, J., 2019. Electro-osmosis treatment techniques and their effect on dewatering of soils, sediments, and sludge: A review. *Soils and Foundations*, 59(2), pp.407-418.

Matsumoto, H. and Tanioka, A., 2011. Functionality in electrospun nanofibrous membranes based on fiber's size, surface area, and molecular orientation. *Membranes*, 1(3), pp.249-264.

MEF., 2007. Government decree on the assessment of soil contamination and remediation needs 214/2007 (legally binding texts are those in Finnish and Swedish Ministry of the Environment).

Micic, S., Shang, J.Q. and Lo, K.Y., 2003. Improvement of the load-carrying capacity of offshore skirted foundations by electrokinetics. *Canadian geotechnical journal*, *40*(5), pp.949-963.

Micic, S., Shang, J.Q., Lo, K.Y., Lee, Y.N. and Lee, S.W., 2001. Electrokinetic strengthening of a marine sediment using intermittent current. *Canadian Geotechnical Journal*, 38(2), pp.287-302.

Mitchell, J.K. and Soga, K., 2005. Fundamentals of soil behavior (Vol. 3). New York: John Wiley & Sons.

Mohamedelhassan, E. and Shang, J.Q., 2001. Effects of electrode materials and current intermittence in electro-osmosis. *Proceedings of the Institution of Civil Engineers-Ground Improvement*, *5*(1), pp.3-11.

Mumtaz, M. and Girish, M.S., 2014. Electrokinetic Geotextile Stabilization Of Embankment Slopes. *International Journal of Engineering Research*, *3*(12), pp.766-768.

Najafabadi, H.H., Irani, M., Rad, L.R., Haratameh, A.H. and Haririan, I., 2015. Removal of Cu2+, Pb2+ and Cr6+ from aqueous solutions using a chitosan/graphene oxide composite nanofibrous adsorbent. *Rsc Advances*, 5(21), pp.16532-16539.

Olivier, J., Conrardy, J.B., Mahmoud, A. and Vaxelaire, J., 2015. Electro-dewatering of wastewater sludge: an investigation of the relationship between filtrate flow rate and electric current. *water research*, *82*, pp.66-77.

Otsuki, N., Yodsudjai, W. and Nishida, T., 2007. Feasibility study on soil improvement using electrochemical technique. *Construction and Building Materials*, *21*(5), pp.1046-1051.

Page, A. L., Miller, R. H. and Keeney, D. R., 1982. Methods of soil analysis. *American Society of Agronomy*.

Patel, K.P., Thakur, L.S. and Shah, D.L., 2021. Effect of Various Factors Affecting Electrokinetics Dewatering of Soil Using Conductive Geotextile. In *Proceedings of the Indian Geotechnical Conference 2019* (pp. 641-652). Springer, Singapore.

Peppicelli, C., Cleall, P., Sapsford, D. and Harbottle, M., 2018. Changes in metal speciation and mobility during electrokinetic treatment of industrial wastes: Implications for remediation and resource recovery. *Science of the total environment*, *624*, pp.1488-1503.

Pugh, R.C., 2002. The application of electrokinetic geosynthetic materials to uses in the construction industry (Doctoral dissertation, Newcastle University).

Qian, X., Zhou, X., Wu, J., Liu, C., Wei, Y. and Liu, J., 2019. Electro-dewatering of sewage sludge: Influence of combined action of constant current and constant voltage on performance and energy consumption. *Science of The Total Environment*, *667*, pp.751-760.

Ramírez, E.M., Camacho, J.V., Rodrigo, M.A. and Cañizares, P., 2015. Combination of bioremediation and electrokinetics for the in-situ treatment of diesel polluted soil: a comparison of strategies. *Science of the Total Environment*, *533*, pp.307-316.

Rao, B., Pang, H., Fan, F., Zhang, J., Xu, P., Qiu, S., Wu, X., Lu, X., Zhu, J., Wang, G. and Su, J., 2021. Pore-scale model and dewatering performance of municipal sludge by ultrahigh pressurized electro-dewatering with constant voltage gradient. *Water Research*, *189*, p.116611.

Reddy, K.R. and Chinthamreddy, S., 2004. Enhanced electrokinetic remediation of heavy metals in glacial till soils using different electrolyte solutions. *Journal of Environmental Engineering*, *130*(4), pp.442-455.

Rittirong, A., Douglas, R.S., Shang, J.Q. and Lee, E.C., 2008. Electrokinetic improvement of soft clay using electrical vertical drains. *Geosynthetics International*, 15(5), pp.369-381.

Rotte, V.M., Sutar, A.A., Patel, A. and Patel, A., 2021. Effect of Various Parameters on Electrokinetic Dewatering of Saturated Clay. In *Proceedings of the Indian Geotechnical Conference 2019* (pp. 183-194). Springer, Singapore.

Shen, Y., Feng, J., Ma, Y. and Liu, H., 2019. Two-dimensional electroosmotic consolidation theory of nonlinear soil voltage distribution characteristics. *Advances in Civil Engineering*, *2019*.

Sun, Z., Zhou, W., Pan, Y. and Shi, G., 2021. Vacuum Preloading Incorporated with Electroosmosis Strengthening of Soft Clay-an Optimized Approach. *Soil Mechanics and Foundation Engineering*, *58*(3), pp.237-243.

Tan, S., Huang, X. and Wu, B., 2007. Some fascinating phenomena in electrospinning processes and applications of electrospun nanofibers. *Polymer International*, 56(11), pp.1330-1339.

Tang, X., Li, Q., Wang, Z., Hu, Y., Hu, Y. and Li, R., 2018. In situ electrokinetic isolation of cadmium from paddy soil through pore water drainage: Effects of voltage gradient and soil moisture. *Chemical Engineering Journal*, *337*, pp.210-219.

Tanioka, A. and Takahashi, M., 2016. Nanofibers. In High-Performance and Specialty Fibers (pp. 273-283). Springer, Tokyo.

Thenmozhi, S., Dharmaraj, N., Kadirvelu, K. and Kim, H.Y., 2017. Electrospun nanofibers: New generation materials for advanced applications. *Materials Science and Engineering*: B, 217, pp.36-48.

Wang, B. and Vu, M.Q., 2010. Improvement of silty clay by vacuum preloading incorporated with electroosmotic method. *Journal of Rock Mechanics and Geotechnical Engineering*, *2*(4), pp.365-372.

Wang, J., Fu, H., Liu, F., Cai, Y. and Zhou, J., 2018. Influence of electro-osmosis activation time on vacuum electro-osmosis consolidation of a dredged slurry. *Canadian Geotechnical Journal*, 55(1), pp.147-153.

Wang, J., Ma, J., Liu, F., Mi, W., Cai, Y., Fu, H. and Wang, P., 2016. Experimental study on the improvement of marine clay slurry by electroosmosis-vacuum preloading. *Geotextiles and Geomembranes*, *44*(4), pp.615-622.

Wang, L., Huang, P., Liu, S. and Alonso, E., 2020. Analytical solution for nonlinear consolidation of combined electroosmosis-vacuum-surcharge preloading. *Computers and Geotechnics*, *121*, p.103484.

Wu, B., Dai, X. and Chai, X., 2020. Critical review on dewatering of sewage sludge: Influential mechanism, conditioning technologies and implications to sludge re-utilizations. *Water research*, *180*, p.115912.

Wu, H., Qi, W., Hu, L. and Wen, Q., 2017. Electro-osmotic consolidation of soil with variable compressibility, hydraulic conductivity and electro-osmosis conductivity. *Computers and Geotechnics*, *85*, pp.126-138.

Wu, P., Shi, Y., Wang, Z., Xiong, Z., Liu, D., Gerson, A.R. and Pi, K., 2019. Effect of electric field strength on electro-dewatering efficiency for river sediments by horizontal electric field. *Science of the total environment*, *647*, pp.1333-1343.

Wu, Y., Xu, Y., Zhang, X., Lu, Y., He, X., Song, B., Zhang, Y. and Ji, J., 2020. Experimental study on treating landfill sludge by preconditioning combined with vacuum preloading: Effects of freeze-thaw and FeCl3 preconditioning. *Science of the Total Environment*, 747, p.141092.

Xiao, F., Guo, K. and Zhuang, Y.F., 2021. Study on electroosmotic consolidation of sludge using EKG. *International Journal of Geosynthetics and Ground Engineering*, *7*(2), pp.1-11.

Xu, H., Zhao, P., Ran, Q., Li, W., Wang, P., Luo, Y., Huang, C., Yang, X., Yin, J. and Zhang, R., 2021. Enhanced electrokinetic remediation for Cd-contaminated clay soil by addition of nitric acid, acetic acid, and EDTA: Effects on soil micro-ecology. *Science of The Total Environment*, *772*, p.145029.

Yang, X., Xie, Y., Dong, J., Liu, G. and Zheng, Y., 2021. Study on Electroosmosis Consolidation of Punctiform Electrode Unit. *Advances in Materials Science and Engineering*, *2021*.

Yip, T.C., Tsang, D.C., Ng, K.T. and Lo, I.M., 2009. Empirical modeling of heavy metal extraction by EDDS from single-metal and multi-metal contaminated soils. *Chemosphere*, 74(2), pp.301-307.

Zhang, H., Zhou, G., Zhong, J., Shen, Z. and Shi, X., 2017. Effect of nanomaterials and electrode configuration on soil consolidation by electroosmosis: experimental and modeling studies. *Rsc Advances*, *7*(20), pp.12103-12112.

Zhang, L. and Hu, L., 2019. Laboratory tests of electro-osmotic consolidation combined with vacuum preloading on kaolinite using electrokinetic geosynthetics. *Geotextiles and Geomembranes*, *47*(2), pp.166-176.

Zhang, L., Pan, Z., Wang, B., Fang, C., Chen, G., Zhou, A., Jiang, P. and Wang, L., 2021. Experimental investigation on electro-osmotic treatment combined with vacuum preloading for marine clay. *Geotextiles and Geomembranes*, *49*(6), pp.1495-1505.

Zhang, W., He, Z., Han, Y., Jiang, Q., Zhan, C., Zhang, K., Li, Z. and Zhang, R., 2020. Structural design and environmental applications of electrospun nanofibers. *Composites Part A: Applied Science and Manufacturing*, 137, p.106009.

Zhang, X., Lu, Y., Yao, J., Wu, Y., Tran, Q.C. and Vu, Q.V., 2020. Insight into conditioning landfill sludge with ferric chloride and a Fenton reagent: Effects on the consolidation properties and advanced dewatering. *Chemosphere*, *252*, p.126528.

Zhang, Y., Cao, B., Ren, R., Shi, Y., Xiong, J., Zhang, W. and Wang, D., 2021. Correlation and mechanism of extracellular polymeric substances (EPS) on the effect of sewage sludge electro-dewatering. *Science of The Total Environment*, *801*, p.149753.

Zhou, J., Tao, Y.L., Xu, C.J., Gong, X.N. and Hu, P.C., 2015. Electro-osmotic strengthening of silts based on selected electrode materials. *Soils and Foundations*, *55*(5), pp.1171-1180.

Zhuang, Y.F. and Wang, Z., 2007. Interface electric resistance of electroosmotic consolidation. *Journal of Geotechnical and Geoenvironmental Engineering*, *133*(12), pp.1617-1621.

Zhuang, Y.F., 2021. Large scale soft ground consolidation using electrokinetic geosynthetics. *Geotextiles and Geomembranes*, *49*(3), pp.757-770.

Zhuang, Y.F., Huang, Y., Liu, F., Zou, W. and Li, Z., 2014, September. Case study on hydraulic reclaimed sludge consolidation using electrokinetic geosynthetics. In *10th international conference on geosynthetics, Berlin, Germany (CD-ROM)*.